Supporting Information

Proton Conduction in a Phosphonate-based Metal-Organic Framework Mediated by Intrinsic "Free Diffusion Inside a Sphere"

Simona Pili,[1] Stephen P. Argent,[2] Christopher G. Morris,[2,3] Peter Rought,[1] Victoria García-Sakai,[4] Ian P. Silverwood,[4] Timothy L. Easun,[5] Ming Li,[6] Mark R. Warren,[3] Claire Murray,[3] Chiu C. Tang,[3] Sihai Yang,[1]* and Martin Schröder[1]*

[1] School of Chemistry, University of Manchester, Oxford Road, Manchester, M13 9PL (UK)
E-mail: Sihai.Yang@manchester.ac.uk; E-mail: M.Schroder@manchester.ac.uk

[2] School of Chemistry, University of Nottingham, University Park, Nottingham NG7 2RD (UK)

[3] Diamond Light Source, Harwell Science Campus, Oxfordshire, OX11 0DE (UK)

[4] ISIS Neutron Facility, STFC Rutherford Appleton Laboratory, Chilton, Oxfordshire, OX11 0QX (UK)

[5] School of Chemistry, Cardiff University, Cardiff, CF10 3XQ (UK)

[6] Department of Mechanical, Materials and Manufacturing Engineering, University of Nottingham, University Park, Nottingham NG7 2RD (UK)

Materials and General Characterisations

$Ni(NO_3)_2 \cdot 6H_2O$ (99%) was purchased from Acros Organics and $Co(NO_3)_2 \cdot 6H_2O$ (98%) from Sigma Aldrich, and both were used without further purification. Elemental analyses for C, H, and N were performed on a CE-440 Elemental Analyser. The FTIR spectra were collected on a Thermo Scientific Nicolet iS5-IR spectrometer in the 4000-400 cm^{-1} range, and thermogravimetric analyses (TGA) were recorded on a Pyris 1 TGA thermogravimetric analyser (Perkin Elmer) under N_2 (60-100 ml/min) with a heating rate of 5 $^oC\ min^{-1}$. Solid state UV-vis spectra were collected on an Ocean Optics USB2000+UV-VIS-ES spectrometer using a DT-MINI-2-GS light source and an R-400-7 fibre optic reflectance probe. Spectra were collected in reflectance (R) mode and converted to F(R) using the Kubelka-Munk function.[1] High resolution (HR) and *in situ* variable temperature (VT) synchrotron powder X-ray diffraction (PXRD) data were collected on Beamline I11 at Diamond Light Source using a multi-analysing crystal (MAC) detector and monochromated radiation (λ = 0.8269 Å). For the measurements, the samples were loaded in a capillary of diameter of 0.5 mm attached to a gas-cell system.

Crystal Structure Determination. The diffraction data for MFM-500(Ni) and MFM-500(Co) were collected at Diamond Light Source, Beamline I19, on a CrystalLogic Kappa 4-circle diffractometer equipped with a Rigaku Saturn 724+CCD detector using synchrotron radiation with a wavelength of 0.6889 Å. Crystals were mounted under a film of Fomblin perfluoropolyether on a Mitegen Micromount and flash frozen under the cold stream of the diffractometer. The raw data were reduced and corrected for Lorentz and polarisation effects using CrystalClear (Rigaku, 2010) and corrected for the effects of adsorption using Scale implemented in CrystalClear (Rigaku, 2010). The structures were solved by direct methods and refined by full-matrix least-squares using the SHELXTL software package.[2]

Experimental Details of Refinement of MFM-500(Co). The hydrogen atoms of the phenyl rings on the ligand were placed geometrically and refined with a riding model. Peaks were observed in the electron difference map corresponding to the hydrogen atoms of the bridging coordinated water molecules (O1W, O2W) and the phosphonate hydroxy oxygen atom O33. These electron density peaks were assigned as hydrogen atoms and appropriate restraints applied to their geometries before their positions were allowed to

refine (DFIX). The isotropic displacement parameters for these atoms were fixed at values 1.5 x Uiso of their parent oxygen atoms, and the oxygen-hydrogen bond lengths were restrained to have values of 0.84 Å. The intramolecular hydrogen-hydrogen distances in the water molecules were restrained to be 1.37 Å, and the phosphorus-hydrogen distances of the phosphonate hydoxy group were restrained to have values of 1.98 Å. The hydrogen atoms H1WA and H1WB of water molecule O1W were constrained to lie on the same mirror plane as the water oxygen atom O1W. Two electron density peaks were observed at hydroxy oxygen O33, and were modelled as separate disorder components with half occupancy each. The first of these disordered hydrogen atoms H33A is mutually incompatible with its symmetry-generated equivalent (H33A_1...H33A_2 distance 0.89 Å) and so has a negative part number to prevent a clash. The second disordered hydrogen atom H33 is similarly incompatible with water hydrogen atom H2WA with which it makes a close contact (H33...H2WA distance 1.23 Å). The two clashes experienced by disordered hydrogen atoms H33A and H33 make it impossible for all four of the discussed sites to be occupied in a single asymmetric unit. However, it is very likely that further unmodelled disorder of these protons on sites throughout the unit cell permits allowable combinations of these sites to be occupied. Likewise water hydrogen atoms H1WB and H2WB are directed towards spaces in the unit cell where no suitable hydrogen bond acceptor is present: in all of these cases it is likely that contacts and partial proton transfers are made with unmodelled disordered solvent molecules. Parallel proton conductivity studies performed on this material support the notion of high proton mobility and likely associated disorder.

Experimental Details of Refinement of MFM-500(Ni). The hydrogen atoms of the phenyl rings on the ligand and DMSO methyl groups were geometrically placed and refined with a riding model. The expected hydrogen atoms on the bridging water molecules (O1W an O2W) and the phosphonate hydroxy groups (O33 and O34) were not observed in the electron density map and were not included in the model. However, they were included in the unit cell contents.

Impedance Measurements. Impedance analyses were performed on a Solartron SI 1260 Impedance/Gain phase Analyser over a frequency range of 0.1 Hz to 1 MHz at an amplitude of 100 mV and 0 mV DC rest voltage. Temperature and humidity dependent conductivities were determined using an electrochemical cell

equipped with platinum current collectors. The temperature and relative humidity inside the cell was stabilised for 3 h and measured with a Rotronic HC2-C04 probe. Conductivity measurements were carried out on pressed pellets of the finely ground powder samples. Samples for conductivity measurements were prepared by grinding the sample (~0.150 g) into a homogeneous powder with a mortar and pestle, added to a standard 8 mm die, sandwiched between two porous carbon electrodes (Sigracet, GDL 10 BB) to improve contact with the two blocking electrodes, and pressed at 5,000 kg for 5 minutes. Resultant pellets of 8 mm in diameter and a thickness of ~1.30 mm were placed in the electrochemical cell. PXRD data confirm the retention of the framework structure after compression. Electrical measurements were taken at several temperatures and degrees of relative humidity obtained by a continuous flow of water-saturated N_2 through the cell. The proton conductivity (σ, S cm^{-1}) was calculated from the impedance data, using the following equation: $\sigma = l/RS$, where l and S are the thickness (cm) and cross-sectional area (cm^2) of the pellet respectively, and R, which was extracted from the impedance plots, is the total resistance of the sample (Ω). ZView software was used to analyse the impedance data.

Quasi elastic neutron scattering. The dynamics of the protons were probed using the neutron spectrometer IRIS at the ISIS Pulsed Neutron and Muon Source, Chilton, UK; a time-of-flight inverted-geometry crystal analyser spectrometer with diffraction capabilities. In the quasi-elastic neutron scattering (QENS) measurements, neutrons scattered from the sample were energy-analysed by means of Bragg reflections from a single crystal array of pyrolytic graphite in close to the backscattering geometry $2\theta_B = 175^o$, where θ_B is the Bragg angle of the analyser crystal, and were counted in a detector array covering $27^o < 2\theta, 158^o$ yielding a wave vector range of 0.4 $Å^{-1}$ to 1.8 $Å^{-1}$. In this study, IRIS was operated in the PG(002) configuration which provides an energy window of -0.5 meV$<\hbar\omega<$ 0.5 meV and an energy resolution ΔE_{res} of 17.5 μeV. The powdered sample was loaded into an annular aluminium container having a suitable sample thickness to minimise multiple scattering effects.

The QENS data were collected at temperatures between 30 K (for resolution) and 423 K with counting times 6 h at each temperature.

Synthesis of $[Ni_3(H_3L)_2(H_2O)_9(C_2H_6SO)_3]$, MFM-500(Ni).

H_6L (0.0136 g, 0.025 mmol) and $Ni(NO_3)_2 \cdot 6H_2O$ (0.0145 g, 0.05 mmol) were dissolved in water, DMSO and DMF (3.5mL, 1.5:1:1, v/v/v) at room temperature. The clear pale green solution was sealed in a vial and heated on an aluminium heating block at 40 ^oC for 2 days. The product was collected by filtration, washed with DMF and dried in air to afford green hexagonal block single crystals of MFM-500(Ni). Elemental analysis (%): anal. calc. for $C_{54}H_{72}O_{30}S_3P_6Ni_3$: C 39.09, H 4.37, N 0.00; found C 39.76, H 4.33, N 0.76. The small N % observed is assigned to trace amounts of DMF in the sample from the synthesis. IR: ν (cm^{-1}) = 3200m, 2100w, 1620m, 1500w, 1460w, 1270w, 1260w, 1250w, 1120w, 1050s, 890w, 800s, 760m, 700s.

Synthesis of $[Co_3(H_3L)_2(H_2O)_9(C_2H_6SO)_3]$, MFM-500(Co).

The same synthetic conditions as with MFM-500(Ni) were used for the synthesis of MFM-500(Co). The clear pale pink solution was sealed in a vial and heated at 40 ^oC for 1 day. The product was collected by filtration, washed with DMF and dried in air to afford pink hexagonal block single crystals of MFM-500(Co). Elemental analysis (%): anal. calc. for $C_{54}H_{72}O_{30}S_3P_6Co_3$: C 39.07, H 4.37, N 0.00; found C 39.80, H 4.24, N 0.67. The small N % observed is assigned to trace amounts of DMF in the sample from the synthesis. IR: ν (cm^{-1}) = 3200m, 2100w, 1620m, 1500w, 1460w, 1270w, 1260w, 1250w, 1120w, 1050s, 890w, 800s, 760m, 700s.

Crystal structure analysis

Table S1. Single crystal X-ray diffraction experimental details for MFM-500(Ni) and MFM-500(Co).

	MFM-500(Ni)	**MFM-500(Co)**
Empirical formula	$[Ni_3(H_3L)_2(H_2O)_9(C_2H_6SO)_3]_\infty$*	$[Co_3(H_3L)_2(H_2O)_9(C_2H_6SO)_3]_\infty$*
Chemical formula**	$C_{54}H_{72}O_{30}S_3P_6Ni_3$	$C_{54}H_{72}O_{30}S_3P_6Co_3$
M_r	1659.29	1659.97
Temperature, K	120(2)	120(2)
Crystal system	$P6_3/m$	$P6_3/m$
***a* (Å)**	16.323(6)	16.348(9)
***c* (Å)**	14.933(8)	14.922(12)
***α* (°)**	90	90
γ (°)	120	120
Cell volume (Å^3)	3446(3)	3454(5)
Z	2	2
Radiation type	Synchrotron λ = 0.6889 Å	Synchrotron λ = 0.6889 Å
μ (mm^{-1})	1.05	0.96
Crystal size (mm)	0.1 × 0.1 × 0.1	0.1 × 0.1 × 0.1
Absorption correction	Multi-scan (*CrystalClear*-Scale, Rigaku 2010)	Multi-scan (*CrystalClear*-Scale, Rigaku 2010)
T_{min}, T_{max}	0.518, 1.000	0.214, 1.000
No. of measured, independent and observed [$I > 2s(I)$] reflections	20957, 2734, 1462	21352, 2752, 1817
R_{int}	0.132	0.173
$(\sin\theta/\lambda)_{max}$ (Å^{-1})	0.650	0.649
$R[F^2 > 2\sigma(F^2)]$, $wR(F^2)$, S	0.084, 0.263, 0.97	0.086, 0.280, 1.09
No. of reflections	2734	2752
No. of parameters	156	162
No. of restraints	236	335
H-atom treatment	H-atom parameters constrained	H atoms treated by a mixture of independent and constrained refinement
Largest diff. Peak/hole (e Å^{-3})	1.68, -0.62	0.55, -0.91
CCDC numbers	1450011	1450010

*L = $C_{24}H_{15}P_3O_9$

**Chemical formula listed includes disordered atoms not included in the structure model.

Table S2. Summary of the refinement details for the H atoms in MFM-500(Co).*

Type	Atom	Peak	x	y	z	Sof
Refined	H1WB	0.67	0.3515	0.8102	0.25	0.5
Refined	H1WA	0.25	0.2559	0.7567	0.25	0.5
Refined	H2WB	0.6	0.1712	0.5432	0.5784	1
Refined	H2WA	0.45	0.2419	0.5209	0.5715	1
Riding	H12	0.49	0.9616	1.119	0.3774	1
Riding	H22A	0.35	0.8146	1.0604	0.3136	0.491
Riding	H23A	0.49	0.6569	1.0192	0.3228	0.491
Riding	H25A	0.36	0.603	0.7906	0.4686	0.491
Riding	H26A	0.34	0.7585	0.8288	0.4544	0.491
Riding	H22B	0.46	0.8282	1.0705	0.4579	0.509
Riding	H23B	0.38	0.6677	1.0275	0.4691	0.509
Riding	H25B	0.58	0.5906	0.7908	0.3317	0.509
Riding	H26B	0.29	0.7473	0.8297	0.3156	0.509
Refined	H33A	0.5	0.4847	0.9701	0.4976	0.5
Refined	H33	0.38	0.4271	0.8907	0.5163	0.5

*Peak heights and locations were observed at the locations of hydrogen atoms in an electron density omit map of MFM-500(Co) after using an OMIT $H instruction to ignore the contributions of the hydrogen atoms in the structure factor calculation and least squares refinement. The positive peaks confirm the presence of electron density within 0.31 Å of the hydrogen atom positions.

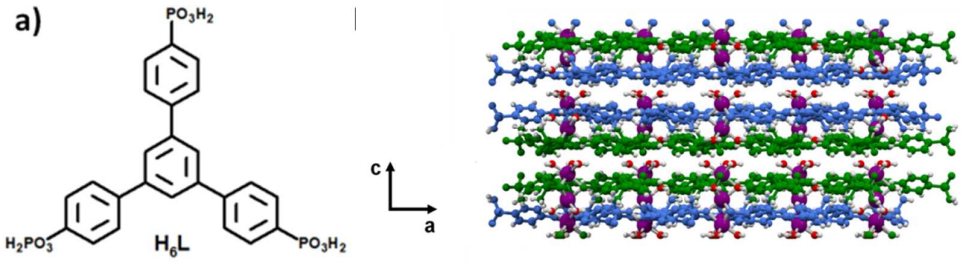

Figure S1. (a) View of the chemical structure of H_6L; (b) views of the crystal structure of MFM-500(M) (M = Co, Ni) along the *b*-axis. Minor disorder component sites and DMSO solvent molecules have been omitted for clarity. Overlapping stacks of ligands blue and green; metal centres purple; bridging water oxygen atoms red; hydrogen atoms white.

Infrared absorption spectroscopy

Figure S2 shows the IR absorption spectra of MFM-500(Ni) and MFM-500(Co). The typical ν(O-H) stretching vibration is observed as a broad band centred at 3200 cm^{-1}. The shoulder centred at 2200 cm^{-1} is attributed to the hydroxyl groups from the phosphonate ν(P-OH). The peaks assigned as the ν(P-O) stretch are observed at 1132 cm^{-1} and 937 cm^{-1}.

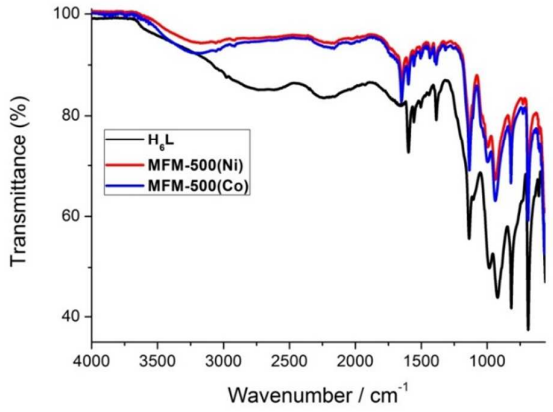

Figure S2. ATR IR spectra of H_6L (*black*), MFM-500(Ni) (*red*) and MFM-500(Co) (*blue*).

Thermogravimetric analysis

TGA plots for as synthesised MFM-500(Ni) with molecular formula $[Ni_3(H_3L)_2(H_2O)_9(C_2H_6SO)_3]$, showed four weight loss steps (Figure S3). The first weight loss step at 75 °C (~10%) is attributed to the loss of 9 molecules of water, to give $[Ni_3(H_3L)_2]$. The dehydrated MOF is stable up to about 220 °C. The following two weight loss steps between 220-650 °C are assigned to the loss of three DMSO molecules (~14 %) and decomposition of the organic ligand (~35 %). The final burning into inorganic phosphonic moieties, $(Ni_3P_6O_9)$, occurs at 700 °C. TGA plots of the isostructural MFM-500(Co) material showed a lower thermal stability of ~23 °C, compared with MFM-500(Ni), and similar weight loss steps.

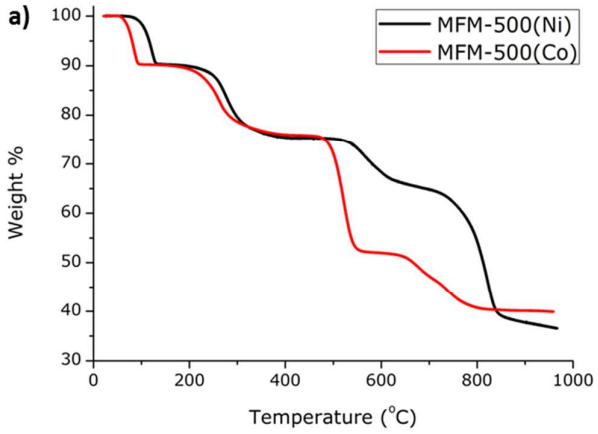

Figure S3. Thermogravimetric profiles of MFM-500(Ni, Co) recorded under N_2 at a heating rate of 5 °C min^{-1}: MFM-500(Ni) (*black*), MFM-500(Co) (*red*).

***In situ* Variable Temperature PXRD**

The temperature dependent synchrotron X-ray powder diffraction patterns for MFM-500(Ni) and MFM-500(Co) are shown in Figures S4 and S5, respectively.

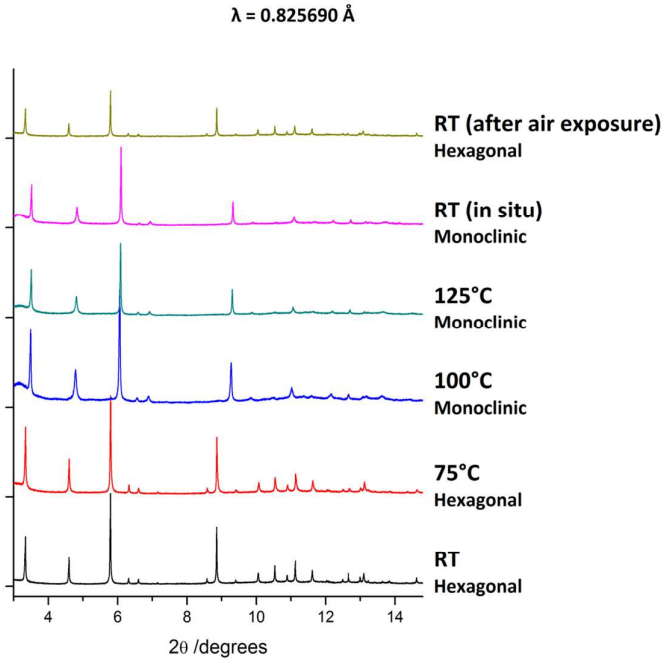

Figure S4. Temperature dependent synchrotron X-ray powder diffraction patterns for MFM-500(Ni).

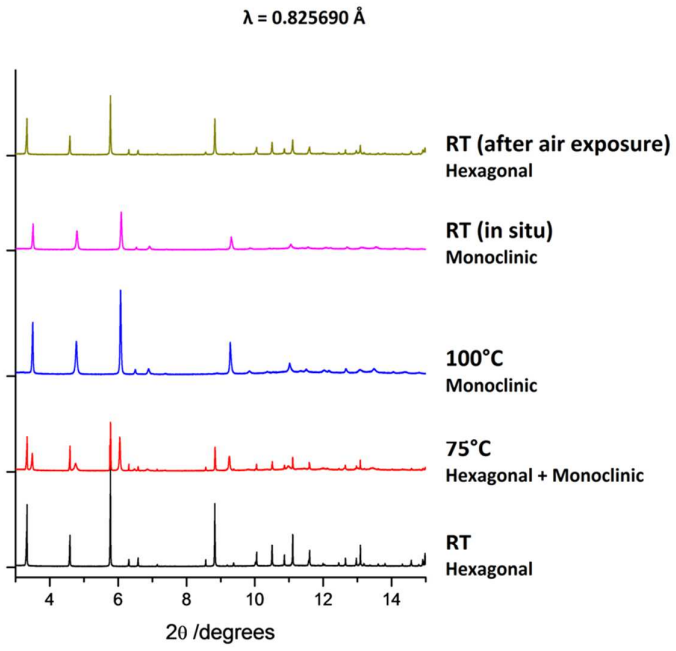

Figure S5. Temperature dependent synchrotron X-ray powder diffraction patterns for MFM-500(Co).

Tables S3 and S4 show the unit cell parameters of the reversible crystallographic phase transition. For MFM-500(Co), at 75 ^{o}C a mixture of the hexagonal and monoclinic phase was observed and the unit cell parameters were extracted separately. The phase transition to the dehydrated phase has gone to completion at 100 ^{o}C and the original phase has disappeared completely. The unit cell parameters of the dehydrated phases were refined accordingly. Due to the quality of the data and the complexity of the structures, attempts to determine the crystal structure of dehydrated phase have thus far been unsuccessful.

Table S3. Unit cell parameters from VT-PXRD study for MFM-500(Co).

Temperature	**RT**	**75 °C**	
Crystal system	Hexagonal	Hexagonal	Monoclinic
Space group	$P6_3/m$	$P6_3/m$	I_a
a	16.3811(1)	16.3696(2)	14.5254(7)
b	16.3811(1)	16.3696(2)	15.6325(3)
c	14.9857(1)	14.9920(2)	30.5329(14)
α	90°	90°	90°
β	90°	90°	117.542(5)°
γ	120°	120°	90°
R_{wp}	9.79	9.57	
GoF	1.58	1.75	
Colour	Pink	indigo	

Temperature	**100 °C**	**RT *in situ***	**RT *ex situ***
Crystal system	Monoclinic	Monoclinic	Hexagonal
Space group	I_a	I_a	$P6_3/m$
a	14.5483(4)	14.4708(5)	16.3813(1)
b	15.5691(4)	15.5183(3)	16.3813(1)
c	30.5100(10)	30.4061(11)	14.9917(1)
α	90°	90°	90°
β	117.854(3)°	117.820(3)°	90°
γ	90°	90°	120°
R_{wp}	7.44	8.60	8.46
GoF	1.87	1.37	1.33
Colour	Blue	Blue	Pink

Table S4. Unit cell parameters from VT-PXRD study for MFM-500(Ni).

Temperature	**RT**	**75 °C**	**100 °C**
Crystal system	Hexagonal	Hexagonal	Monoclinic
Space group	$P6_3/m$	$P6_3/m$	I_a
a	16.3258(2)	16.3052(1)	14.3828(6)
b	16.3258(2)	16.3052(1)	15.5824(3)
c	14.9749(1)	14.9450(2)	30.3991(13)
α	90°	90°	90°
β	90°	90°	117.480(4)°
γ	120°	120°	90°
R_{wp}	8.30	7.29	6.16
GoF	1.44	1.47	1.72
Colour	Green	Green	Brown

Temperature	**125 °C**	**RT *in situ***	**RT *ex situ***
Crystal system	Monoclinic	Monoclinic	Hexagonal
Space group	I_a	I_a	$P6_3/m$
a	14.3514(7)	14.2833(8)	16.3258(2)
b	15.5308(7)	15.5040(4)	16.3258(2)
c	30.3605(13)	30.2818(20)	15.0030(2)
α	90°	90°	90°
β	117.596(4)°	117.494(4)°	90°
γ	90°	90°	120°
R_{wp}	8.42	8.96	8.46
GoF	1.56	1.64	1.32
Colour	Brown	Brown	Green

Proton conductivity study.

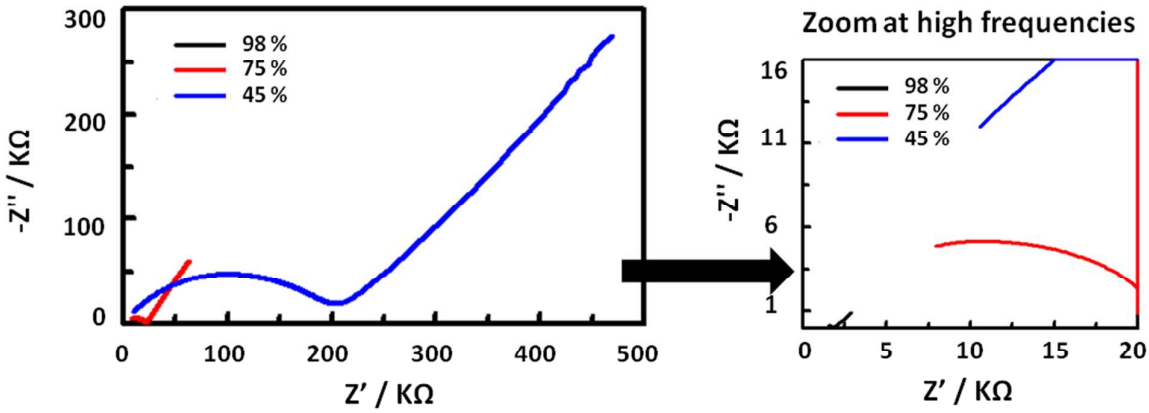

Figure S6. Nyquist plots for MFM-500(Ni) measured at different % RH and room temperature.

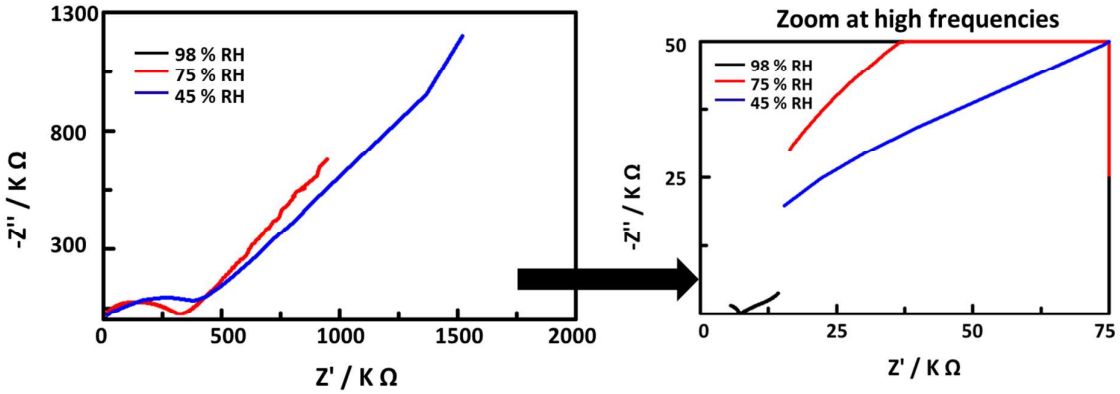

Figure S7. Nyquist plots for MFM-500(Co) measured at different % RH and room temperature.

Table S5. Proton conductivities (S cm^{-1}) for MFM-500(Ni, Co) measured at different % RH and 25 ^{o}C.

Sample	σ at 98 % RH	σ at 75 % RH	σ at 45 % RH	σ at 0 % RH*
MFM-500(Ni)	4.5 x 10^{-4}	1.50 x 10^{-5}	1.58 x 10^{-6}	< 10^{-9}
MFM-500(Co)	4.4 x 10^{-5}	1.00 x 10^{-6}	5.10 x 10^{-7}	< 10^{-9}

* The precise proton conductivities recorded under anhydrous conditions are not reported due to the high resistivity of the materials under these experimental conditions.

Calculation of Activation Energy.

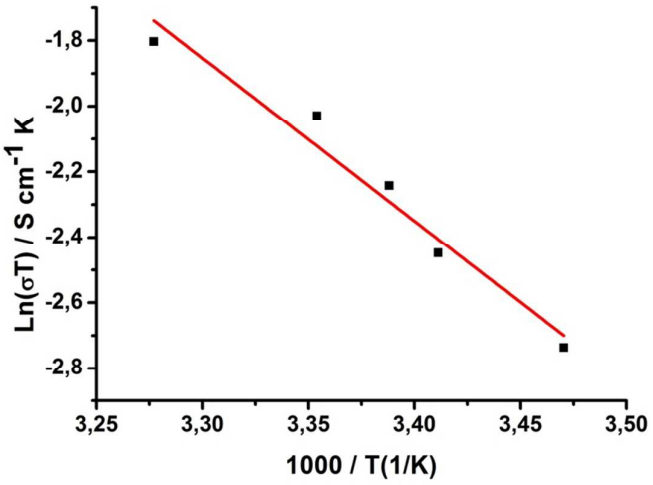

Figure S8. Arrhenius plot of the proton conductivity at various temperatures of MFM-500(Ni) under 98 % RH.

We have carried out impedance measurements in the high temperature region, where the materials undergo dehydration and show negligible proton conductivity. The full proton conductivity can be recovered once the dehydrated samples are re-hydrated.

Solid-state UV-visible absorption spectroscopy

The difference in the conductivities in these isostructural materials probably correlates to the bond strength of coordinated water molecules, as suggested by the different stabilities shown in the TGA plots. To probe this further, solid-state UV-visible absorption spectra were measured (Figure S9, Tables S6 and S7). Single crystals of MFM-500(Ni) and MFM-500(Co) were suspended in dry solvents (methanol, acetonitrile, dichloromethane and benzene) for one week with frequent solvent exchange. UV-visible absorption spectra for MFM-500(Ni) show an absorption band centred at *ca.*410 nm for all solvent-exchanged samples (Figures S9a, Table S6). For dehydrated MFM-500(Ni) after heating at 125 ^{o}C, a significant shift of the absorption band from *ca.* 410 nm to *ca.* 460 nm is observed, consistent with a colour change from green to brown. In contrast, for MFM-500(Co), polar solvents (*i.e.*, methanol and CH_3CN) caused a significant colour change corresponding to the formation of a band centred at 630 nm in the UV-visible spectra, suggesting that the coordinated water can be partially replaced *via* solvent exchange (Figures S9b, Table S7). This result

indicates that the water molecules are more strongly coordinated to the Ni ions and cannot be displaced under these conditions, leading to the difference in the proton conductivity between these two materials. This also confirms the key role of coordinated water molecules in the assembly of proton hopping pathways in the lattice.

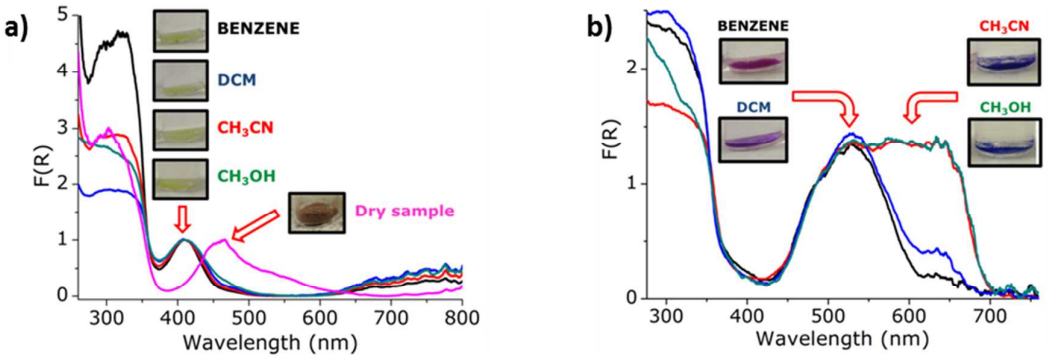

Figure S9. (a) Solid-state UV-visible absorption spectra of MFM-500(Ni) after soaking in dry organic solvents and under vacuum: benzene (*black*); dichloromethane (*blue*); acetonitrile (*red*); methanol (*green*); activated under vacuum (*purple*). (b) Solid-state UV-visible absorption spectra of MFM-500(Co) after soaking in dry organic solvents: benzene (*black*); dichloromethane (*blue*); acetonitrile (*red*); methanol (*green*).

Table S6. Unit cell parameters from HR-PXRD study for MFM-500(Ni) suspended in different dry organic solvents.

Sample	**RT**	**Benzene**	**DCM**	**CH_3CN**	**Activated (125 °C)**
Crystal system	Hexagonal	Hexagonal	Hexagonal	Hexagonal	Monoclinic
Space group	$P6_3/m$	$P6_3/m$	$P6_3/m$	$P6_3/m$	I_a
a	16.3258(2)	16.3228(1)	16.3055(1)	16.3220(1)	14.3514(7)
b	16.3258(2)	16.3228(1)	16.3055(1)	16.3220(1)	15.5308(7)
c	14.9749(1)	14.9581(1)	14.8804(1)	14.9508(1)	30.3605(13)
α	90°	90°	90°	90°	90°
β	90°	90°	90°	90°	117.596(4)°
γ	120°	120°	120°	120°	90°
R_{wp}	8.30	12.92	9.92	9.52	8.42
GoF	1.44	2.32	1.97	1.64	1.56
Colour	Green	Green	Green	Green	Brown

Table S7. Unit cell parameters from HR-PXRD study for MFM-500(Co) suspended in different dry organic solvents.

Sample	RT	Benzene	DCM	CH_3CN
Crystal system	Hexagonal	Hexagonal	Hexagonal	Hexagonal
Space group	$P6_3/m$	$P6_3/m$	$P6_3/m$	$P6_3/m$
a	16.3811(1)	15.7142(11)	16.3585(1)	16.3614(1)
b	16.3811(1)	15.7142(11)	16.3585(1)	16.3614(1)
c	14.9857(1)	14.5526(11)	14.8978(1)	14.8954(1)
α	90°	90°	90°	90°
β	90°	90°	90°	90°
γ	120°	120°	120°	120°
R_{wp}	9.79	12.87	8.76	10.92
GoF	1.58	1.94	13.36	15.93
Colour	Pink	Pink	Lavender	Blue

QENS analysis method.

The QENS data were treated presuming that a significant fraction of protons in MFM-500(Ni) moves slowly for the resolution of the spectrometer; these are the aromatic protons from the organic ligand and those on the methyl group of bound DMSO molecules, and represent the immobile fraction (p). The mobile fraction (1-p) that is constrained to perform the molecular diffusion consists of the protons coming from the water molecules bound to the metal and the free hydroxy from the phosphonate. The function j_0 is the spherical Bessel function, j_1 the first order spherical Bessel function and J_0 the cylindrical Bessel function. Geometrical information of the molecular motions of active protons in MFM-500(Ni) were analysed *via* the elastic incoherent structure factor, EISF.[3]

$$EISF = I_{elastic} / (I_{elastic} + I_{QENS})$$

where $I_{elastic}$ and I_{QENS} are the peak intensities of elastic and quasi-elastic scatterings, respectively. To obtain the elastic ($I_{elastic}$) and QENS (I_{QENS}) intensities, the QENS data were fitted to a Delta function convoluted

with a resolution and a Lorentzian function. The EISF data was fitted using various models with localised diffusive motions (Figure S10).[4-6]

- Jump diffusion between 2 sides: $EISF = p + (1-p) * [(1/2)*(1+j_0(2Qr)]$
- Jump diffusion between 3 sides: $EISF = p + (1-p) * [(1/3)*(1+2j_0(Qr\sqrt{3})]$
- Free diffusion on a circle: $EISF = p + (1-p) * [J_0(Qr)]^2$
- Free diffusion on a spherical surface: $EISF = p + (1-p) * [j_0(Qr)]^2$
- Free diffusion inside a sphere: $EISF = p + (1-p) * [3j_1(Qr)/(Qr)]^2$

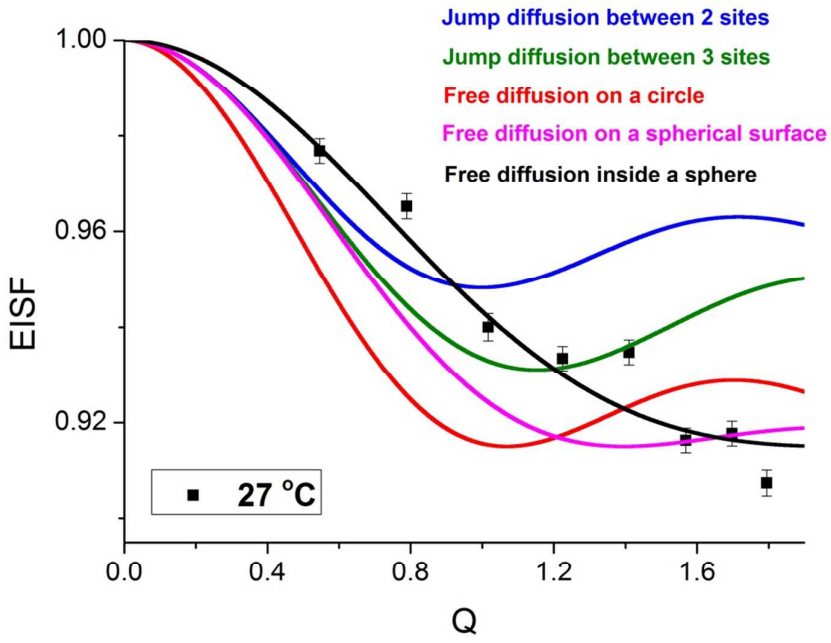

Figure S10. Comparison of the experimental (black squares) and simulated (solid lines) EISF plots for various diffusion models. "Jump diffusion between two sites" (*blue*), "Jump diffusion between three sites" (*green*), "Free diffusion on a circle" (*red*), "Free diffusion on a spherical surface" (*magenta*), "Free diffusion inside a sphere" (*black*). Same *r* distance of 2.25 Å was used for all the fittings for a direct comparison.

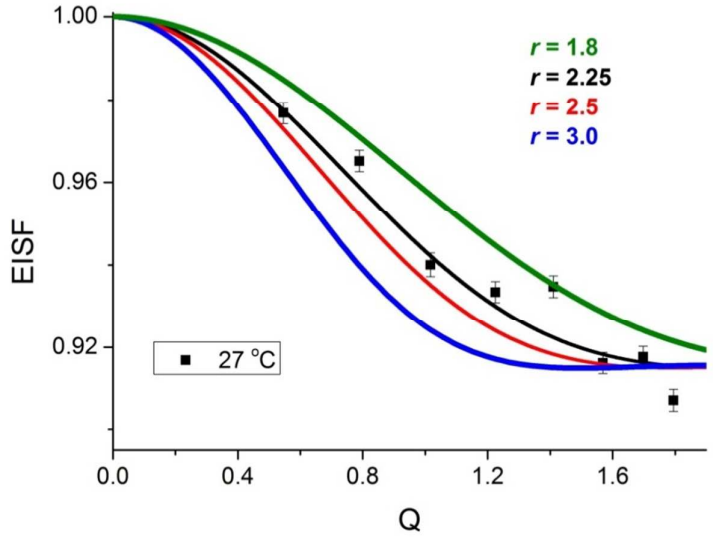

Figure S11. Fitting of the experimental EISF data with the "free diffusion inside a sphere" model using different *r* values.

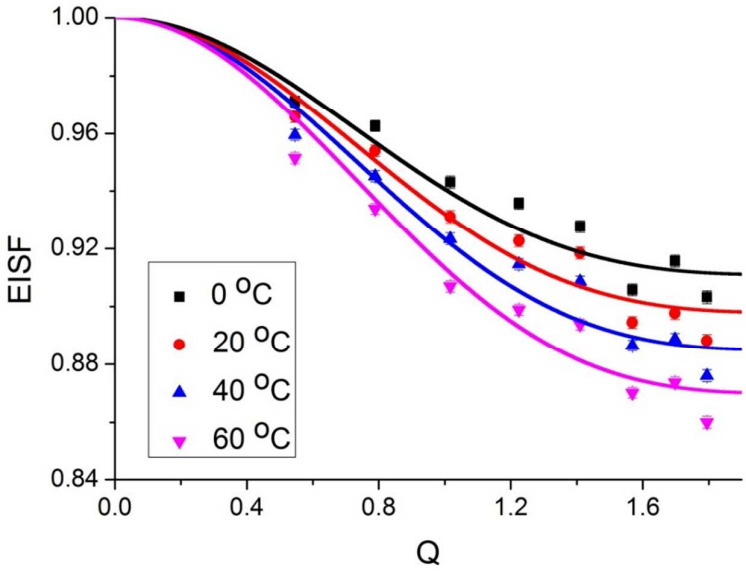

Figure S12. Fitting of the EISF of MFM-500(Ni) under humid conditions with the "free diffusion inside a sphere" model. Solid curves represent the simulated EISF at different temperature and *r* = 2.25Å.

References

1. P. Kubelka, F, Munk, Zeits. *F. Tech. Physic* **1931**, *12*, 589.
2. Sheldrick, G. M. *Acta Cryst.* **2008**, A64, 112-122.
3. Bee, M. "*Quasielastic Neutron Scattering*" **1988**, Adam Hilger, Bristol.
4. Fitter, J.; Gutberlet, T.; Katsaras, J. "*Neutron Scattering in Biology: Techniques and Applications*" **2006**, Springer-Verlag Berlin Heidelberg, New York.
5. Russo, D.; Pérez, J.; Zanotti, J.-M.; Desmadril, M.; Durand, D. *Biophys. J.* **2002**, *83*, 2792–2800.
6. Volino, F.; Dianoux, A. *J., Mol. Phys.* **1980**, *41*, 271. "